

Model order reduction techniques for the stochastic finite volume method

Ray Qu^{1*}, Jesse Chan¹ and Svetlana Tokareva²

¹Department of Computational Applied Mathematics and Operations Research, Rice University, 6100 Main St MS-134, Houston, TX, US, 77005.

²Theoretical Division, Los Alamos National Laboratory, MS B284, Los Alamos, NM, US, 87545.

*Corresponding author(s). E-mail(s): Ray.Qu@rice.edu;
Contributing authors: Jesse.Chan@rice.edu; tokareva@lanl.gov;

Abstract

The stochastic finite volume method (SFV method) is a high-order accurate method for uncertainty quantification (UQ) in hyperbolic conservation laws. However, the computational cost of SFV method increases for high-dimensional stochastic parameter spaces due to the curse of dimensionality. To address this challenge, we incorporate interpolation-based reduced order modeling (ROM) techniques that reduce the cost of computing stochastic integrals in the SFV method. Further efficiency gains are achieved through hyper-reduction with a QR factorization-based Discrete Empirical Interpolation Method (Q-DEIM). Numerical experiments suggest that this approach can lower both computational cost and memory requirements for high-dimensional stochastic parameter spaces.

Keywords: reduced order modeling, uncertainty quantification, stochastic finite volume method

1 Introduction

Hyperbolic systems of partial differential equations are ubiquitous in physics and engineering, where mathematical models are represented by a set of transport-dominated (hyperbolic) balance laws. Many efficient numerical methods have been developed

to approximate the solutions of systems of conservation laws [1, 2], e.g. finite volume schemes [3] or discontinuous Galerkin methods [4–6]. The classical assumption in designing efficient numerical methods for hyperbolic systems is that the initial data, boundary conditions, and coefficients of the model are known exactly, i.e., they are deterministic. However, in many practical applications it is not always possible to obtain exact data due to, for example, measurement, prediction, or modeling errors.

It is well known that solutions to hyperbolic PDEs may develop discontinuities in finite time even from smooth initial data [7, 8]. In the context of stochastic hyperbolic PDEs (SPDEs), this leads to the propagation of discontinuities in both physical and stochastic dimensions, posing significant challenges on the numerical approximation of SPDEs.

Numerical techniques have been developed to quantify uncertainty by computing the mean flow and its statistical moments. They are based on approaches such as Monte Carlo (MC) [9], multilevel Monte Carlo (MLMC) [10], generalized polynomial chaos (gPC) [11, 12], the probabilistic collocation method (PCM) [13], Godunov schemes [14], multiresolution methods [15] and stochastic Galerkin (sG) projections [16, 17].

Uncertainty quantification methods can be roughly classified into intrusive and non-intrusive schemes. *Non-intrusive* UQ methods allow reuse of an existing deterministic code as a black box without any modifications [9, 10, 13, 18–20]. An example of such an approach is the Monte Carlo method [9, 10]: given a large number of realizations of the random parameters, we generate the corresponding outputs from our deterministic code and then process these data to obtain the statistical mean and variances. The possibility to reuse existing deterministic codes is a clear advantage of non-intrusive approaches. However, methods such as Monte Carlo tend to require a prohibitively large number of evaluations of the deterministic solutions. In contrast, *intrusive* UQ methods require modifications to the algorithms and their implementations in the deterministic computational scheme [11, 12, 14–17, 21]. For example, a well-known and widely used sG method for hyperbolic systems transforms the original PDEs for the primary variables into a set of PDEs that are defined with respect to the polynomial expansion coefficients [16]. This reduces the simulation time but might pose mathematical challenges, such as the loss of hyperbolicity of the transformed PDEs.

Recently, we have developed a semi-intrusive Stochastic Finite Volume (SFV) method [22] to quantify uncertainties that arise due to random model parameters in the underlying hyperbolic PDE system, including initial conditions, uncertain constants, and complex time-dependent distributions on boundary conditions. The SFV method requires some modifications of the deterministic code that is used for solving a standard initial boundary value problem (IBVP) for hyperbolic conservation laws, which only involve additional integration of the numerical fluxes over the cells in the stochastic space and can therefore be considered mild. This approach preserves the hyperbolicity of the model and, at the same time, is more computationally efficient than the Monte Carlo method.

The main bottleneck in applying the SFV method to high-dimensional SPDEs is *curse of dimensionality*: an exponential growth of algorithmic complexity and memory

requirements with an increasing number of stochastic dimensions. Several promising approaches have been proposed to improve the scalability of SFV: an adaptive SFV [23] and low-rank Tensor-Train SFV [24].

In this paper, we explore the interpolation-based reduced-order modeling (ROM) techniques that reduce the cost of computing stochastic integrals in the SFV method. Further efficiency gains from hyper-reduction are achieved through the Discrete Empirical Interpolation Method (DEIM) [25] with node selection via the QR factorization with column pivoting, known as Q-DEIM [26].

This paper is organized as follows: Section 2 reviews the SFV method for conservation laws in a one-dimensional physical space. Section 3 presents and compares two reconstruction strategies within the framework of the SFV method. Section 4 applies an interpolation-based reduced-order modeling technique. Section 5 provides numerical experiments for Burgers' and compressible Euler equations that assess the performance of the proposed approach.

2 Stochastic finite volume method

Our work considers the stochastic hyperbolic systems of conservation laws under a one-dimensional spatial domain and q -dimensional parametrized probability space, which is given by the parametric form:

$$\begin{aligned} \partial_t \mathbf{u} + \partial_x \mathbf{F}(\mathbf{u}, \mathbf{y}) &= \mathbf{0}, & x \in D_x \subset \mathbb{R}, & \quad \mathbf{y} \in D_y \subset \mathbb{R}^q, & \quad t > 0; \\ \mathbf{u}(x, 0, \mathbf{y}) &= \mathbf{u}_0(x, \mathbf{y}), & x \in D_x \subset \mathbb{R}, & \quad \mathbf{y} \in D_y \subset \mathbb{R}^q, \end{aligned} \quad (1)$$

where $\mathbf{u} = [u_1, \dots, u_n]^T$, $\mathbf{F} = [f_1, \dots, f_n]^T$.

Let $\cup_{i=1}^{N_x} K_x^i$ be the partition of the computational domain D_x , each with length $|K_x^i|$, and $\cup_{j=1}^{N_y} K_y^j$ be the Cartesian grid in the domain D_y . We further assume the existence of the probability density function $\mu(\mathbf{y})$ and compute the expectation of the p -th solution component of (1) as

$$\mathbb{E}[u_p] = \int_{D_y} u_p \mu(\mathbf{y}) d\mathbf{y}, \quad p = 1, \dots, n.$$

The SFV method can be obtained by integrating (1) over physical-stochastic control volume $K_x^i \times K_y^j$:

$$\int_{K_y^j} \int_{K_x^i} \partial_t \mathbf{u} \mu(\mathbf{y}) dx d\mathbf{y} + \int_{K_y^j} \int_{K_x^i} \partial_x \mathbf{F}(\mathbf{u}, \mathbf{y}) \mu(\mathbf{y}) dx d\mathbf{y} = \mathbf{0}.$$

Introducing the cell average and stochastic cell measure

$$\mathbf{U}_{i,j}(t) = \frac{1}{|K_x^i| |K_y^j|} \int_{K_y^j} \int_{K_x^i} \mathbf{u}(x, t, \mathbf{y}) \mu(\mathbf{y}) dx d\mathbf{y}, \quad |K_y^j| = \int_{K_y^j} \mu(\mathbf{y}) d\mathbf{y}$$

and performing the partial integration over K_x^i , we get

$$\frac{dU_{i,j}}{dt} + \frac{1}{|K_x^i||K_y^j|} \int_{K_y^j} \left[\int_{\partial K_x^i} \mathbf{F}(\mathbf{u}) \cdot \mathbf{n} dS \right] \mu(\mathbf{y}) d\mathbf{y} = \mathbf{0}.$$

Next, we approximate the flux over cell boundaries $\mathbf{F}(\mathbf{u}) \cdot \mathbf{n}$ with a numerical flux

$$\widehat{\mathbf{F}}(\tilde{\mathbf{u}}_L(x, t, \mathbf{y}), \tilde{\mathbf{u}}_R(x, t, \mathbf{y})),$$

where $\tilde{\mathbf{u}}_{L,R}$ denote the reconstructed solution values at the edges of K_x^i . For simplicity of notation, we omit the time t for the remainder of this work. We further denote $\widehat{\mathbf{F}}_{i\pm\frac{1}{2}}$ as the values of $\widehat{\mathbf{F}}$ at the left ($i - \frac{1}{2}$) and right ($i + \frac{1}{2}$) edges of each spatial cell K_x^i . The numerical flux integral can then be simplified into the following integral over stochastic space:

$$\overline{\mathbf{F}}_{i\pm\frac{1}{2},j} = \int_{K_y^j} \widehat{\mathbf{F}}_{i\pm\frac{1}{2}} \mu(\mathbf{y}) d\mathbf{y}. \quad (2)$$

The SFV method then solves the following ODE system:

$$\frac{dU_{i,j}}{dt} + \frac{\overline{\mathbf{F}}_{i+\frac{1}{2},j} - \overline{\mathbf{F}}_{i-\frac{1}{2},j}}{|K_x^i||K_y^j|} = \mathbf{0}, \quad (3)$$

for all $i = 1, \dots, N_x, j = 1, \dots, N_y$.

We can also write the SFV method in matrix form. Let $\overline{\mathbf{F}}_{\pm\frac{1}{2}}$ denote matrices with entries

$$\left(\overline{\mathbf{F}}_{\pm\frac{1}{2}} \right)_{i,j} = \overline{\mathbf{F}}_{i\pm\frac{1}{2},j}.$$

We can then rewrite (3) as

$$\mathbf{M} \frac{d\mathbf{U}}{dt} + \left(\overline{\mathbf{F}}_{+\frac{1}{2}} - \overline{\mathbf{F}}_{-\frac{1}{2}} \right) = \mathbf{0}, \quad (4)$$

where \mathbf{U} is the matrix of cell averages, $\overline{\mathbf{F}}_{\pm\frac{1}{2}}$ denotes the flux integrals over the physical cell boundaries, and \mathbf{M} is a mass matrix such that

$$\left(\mathbf{M} \frac{d\mathbf{U}}{dt} \right)_{i,j} = |K_x^i||K_y^j| \frac{dU_{i,j}}{dt}.$$

Remark 1 While we focus on one-dimensional spatial domains in this work, the SFV method framework extends naturally to systems in two/three-dimensional spatial domains [22].

3 WENO reconstruction

To achieve high-order accuracy, we use a Weighted Essentially Non-Oscillatory (WENO) reconstruction [27, 28] in both the physical and stochastic spaces [22, 29].

We propose two different procedures for reconstructing the numerical flux: WENO with reconstructed states or with reconstructed fluxes. Both of these procedures begin by applying third-order WENO reconstruction in the physical domain to obtain the reconstructed left and right solution states $\tilde{\mathbf{u}}_{L,i\pm\frac{1}{2},j}$, $\tilde{\mathbf{u}}_{R,i\pm\frac{1}{2},j}$ at the physical boundaries of the cell K_x^i . To simplify the presentation, we consider a uniform grid, so that each cell K_x^i has the same size Δx .

Specifically, for each physical cell K_x^i with a solution average $U_{i,j}$ for a fixed index j , we define a three-point stencil with its neighboring solution averages $U_{i\pm 1,j}$. Next, we define candidate linear reconstructions:

$$p_0(x) = U_{i,j} + \frac{U_{i+1,j} - U_{i,j}}{\Delta x}(x - x_i), \quad p_1(x) = U_{i,j} + \frac{U_{i,j} - U_{i-1,j}}{\Delta x}(x - x_i),$$

so that the reconstructed states $\tilde{\mathbf{u}}_{R,i-\frac{1}{2},j}$ and $\tilde{\mathbf{u}}_{L,i+\frac{1}{2},j}$ are defined as a weighted combination of candidate reconstructions at the cell interfaces:

$$\begin{aligned} \tilde{\mathbf{u}}_{R,i-\frac{1}{2},j} &= \omega_0 p_0(x_{i-\frac{1}{2}}) + \omega_1 p_1(x_{i-\frac{1}{2}}), \\ \tilde{\mathbf{u}}_{L,i+\frac{1}{2},j} &= \omega_0 p_0(x_{i+\frac{1}{2}}) + \omega_1 p_1(x_{i+\frac{1}{2}}). \end{aligned}$$

To adaptively determine the contribution of these candidate reconstructions and assign higher weights to smoother stencils, we compute the smoothness indicators:

$$\beta_0 = (U_{i+1,j} - U_{i,j})^2, \quad \beta_1 = (U_{i,j} - U_{i-1,j})^2.$$

The corresponding nonlinear weights are given by

$$\alpha_k = \frac{d_k}{(\epsilon + \beta_k)^2}, \quad \omega_k = \frac{\alpha_k}{\alpha_0 + \alpha_1}, \quad k = 0, 1, \quad (5)$$

where ϵ is a small parameter to prevent division by zero and d_k are linear weights determined by the positions of boundaries of K_x^i . In our implementation, $d_0 = \frac{1}{3}$, $d_1 = \frac{2}{3}$ for the left interface $x_{i-\frac{1}{2}}$ and $d_0 = \frac{2}{3}$, $d_1 = \frac{1}{3}$ for the right interface $x_{i+\frac{1}{2}}$. The reconstructed states, $\tilde{\mathbf{u}}_{R,i-\frac{1}{2},j}$ and $\tilde{\mathbf{u}}_{L,i+\frac{1}{2},j}$, are then computed as

$$\begin{aligned} \tilde{\mathbf{u}}_{R,i-\frac{1}{2},j} &= \omega_0 \left(U_{i,j} - \frac{1}{2} (U_{i+1,j} - U_{i,j}) \right) + \omega_1 \left(U_{i,j} - \frac{1}{2} (U_{i,j} - U_{i-1,j}) \right), \\ \tilde{\mathbf{u}}_{L,i+\frac{1}{2},j} &= \omega_0 \left(U_{i,j} + \frac{1}{2} (U_{i+1,j} - U_{i,j}) \right) + \omega_1 \left(U_{i,j} + \frac{1}{2} (U_{i,j} - U_{i-1,j}) \right). \end{aligned} \quad (6)$$

The remaining two reconstructed states, $\tilde{\mathbf{u}}_{R,i+\frac{1}{2},j}$ and $\tilde{\mathbf{u}}_{L,i-\frac{1}{2},j}$, can be obtained by applying the same procedure to physically neighboring cells.

Remark 2 The formal third-order accuracy of the WENO scheme is achieved only for smooth solutions; in the presence of shocks, the order of accuracy drops to first order [22, 29].

Remark 3 For n -component solutions, WENO reconstruction can be applied independently to each component. In the case of systems in two/three-dimensional physical space, the reconstruction can be performed dimension-by-dimension, as described in [28].

3.1 WENO with reconstructed states

Assuming that we have obtained the reconstructed states $\tilde{\mathbf{u}}_{L,i\pm\frac{1}{2},j}$, $\tilde{\mathbf{u}}_{R,i\pm\frac{1}{2},j}$, the first procedure, as used in [22, 29], is WENO with “reconstructed states” that extends the reconstruction process over the stochastic domain.

This is also performed in a cell-by-cell and dimension-by-dimension manner, following a similar procedure as in (6). As a result, we obtain interpolation polynomials $\tilde{\mathbf{u}}_{L,i\pm\frac{1}{2},j}(\mathbf{y})$, $\tilde{\mathbf{u}}_{R,i\pm\frac{1}{2},j}(\mathbf{y})$ for each $K_x^i \times K_y^j$, which enable the evaluation of approximated solution states at arbitrary quadrature nodes.

For any chosen quadrature rule within one stochastic cell, let $\hat{\mathbf{y}}_m$ and w_m be the corresponding quadrature nodes and weights, respectively.¹ Using this quadrature rule, we approximate the flux integrals in (2) as

$$\int_{K_y^j} \hat{\mathbf{F}}_{i\pm\frac{1}{2}}(\mathbf{y}) \mu(\mathbf{y}) d\mathbf{y} \approx \sum_m \hat{\mathbf{F}}\left(\tilde{\mathbf{u}}_{L,i\pm\frac{1}{2},j}(\hat{\mathbf{y}}_m), \tilde{\mathbf{u}}_{R,i\pm\frac{1}{2},j}(\hat{\mathbf{y}}_m)\right) \mu(\hat{\mathbf{y}}_m) w_m. \quad (7)$$

Since we employ a third-order WENO reconstruction, integrals of numerical fluxes are approximated using two-point Gauss quadrature rules which are exact for cubic polynomials.

3.2 WENO with reconstructed fluxes

The second procedure, WENO with “reconstructed fluxes”, first computes the flux at each cell interface using the reconstructed states:

$$\hat{\mathbf{F}}_{i\pm\frac{1}{2},j}(\mathbf{y}) = \hat{\mathbf{F}}\left(\tilde{\mathbf{u}}_{L,i\pm\frac{1}{2},j}, \tilde{\mathbf{u}}_{R,i\pm\frac{1}{2},j}\right).$$

Then, rather than reconstructing the solution states over the stochastic domain as in the previous procedure, we directly reconstruct the computed flux. This process yields the flux interpolation polynomials $\hat{\mathbf{F}}_{i\pm\frac{1}{2},j}(\mathbf{y})$ for each $K_x^i \times K_y^j$, which can be evaluated at quadrature nodes. Using the same quadratures described in Section 3.1, the flux integrals in (2) are then approximated as

$$\int_{K_y^j} \hat{\mathbf{F}}_{i\pm\frac{1}{2}}(\mathbf{y}) \mu(\mathbf{y}) d\mathbf{y} \approx \sum_m \hat{\mathbf{F}}_{i\pm\frac{1}{2},j}(\hat{\mathbf{y}}_m) \mu(\hat{\mathbf{y}}_m) w_m. \quad (8)$$

A key distinction of this method is that it evaluates the numerical flux only in the physical domain, whereas the reconstructed states procedure requires flux evaluations at every quadrature node in the stochastic domain. Specifically, at each ODE time step, the procedure of reconstructed states requires 2^q times the flux evaluations

¹Note that quadrature weights w_m are distinct from WENO weights ω_k .

compared to the procedure of reconstructed fluxes. This implies if the flux evaluation is a significant part of the computational cost compared to the reconstruction, the procedure of reconstructed fluxes will be more efficient. Such reduction comes from the fact that two-point Gaussian quadrature rule yields 2^q quadrature points in q dimensions. Although the total number of time steps depends on the specific time integrator and CFL condition [30], we observe that this procedure significantly reduces the overall runtime of the ODE time-stepping process in practice when N_y is relatively small, such that each timestep's cost is dominated by flux evaluations rather than nonlinear reconstructions.

4 Reduced stochastic basis

Despite potential runtime improvements with the procedure of reconstructed fluxes, both WENO reconstruction procedures still require evaluating the flux at every quadrature node, resulting in an exponential increase in runtime and memory as the stochastic dimension q grows. To alleviate this, we apply interpolation-based reduced order model (ROM) techniques to reduce costs associated with high dimensional stochastic domains. More specifically, we non-intrusively construct a data-driven reduced basis in the stochastic domain, which allows us to approximate high dimensional stochastic integrals in terms of precomputed operators acting on the reduced stochastic basis.

4.1 Approximating stochastic integrals

We approximate stochastic flux integrals in (2) by representing the flux using N reduced stochastic basis functions $\boldsymbol{\phi}(\mathbf{y}) = [\phi_1(\mathbf{y}), \dots, \phi_N(\mathbf{y})]^T$:

$$\widehat{\mathbf{F}}_{i \pm \frac{1}{2}}(\mathbf{y}) \approx \sum_{k=1}^N \mathbf{c}_{i \pm \frac{1}{2}, k} \phi_k(\mathbf{y}),$$

where $\mathbf{c}_{i \pm \frac{1}{2}, k} \in \mathbb{R}^n$ is a vector of coefficients for the k -th basis at the physical interfaces $i \pm \frac{1}{2}$; each entry in this vector corresponds to the same solution component as the respective entry in $\widehat{\mathbf{F}}_{i \pm \frac{1}{2}}$. The explicit forms of the basis functions can be polynomials or data-driven basis functions such as POD modes, which will be discussed in Sec 4.3. Substituting this expansion into (2), the flux integral transforms into

$$\begin{aligned} \int_{K_y^j} \widehat{\mathbf{F}}_{i \pm \frac{1}{2}}(\mathbf{y}) \mu(\mathbf{y}) d\mathbf{y} &\approx \int_{K_y^j} \sum_{k=1}^N \mathbf{c}_{i \pm \frac{1}{2}, k} \phi_k(\mathbf{y}) \mu(\mathbf{y}) d\mathbf{y} \\ &= \sum_{k=1}^N \mathbf{c}_{i \pm \frac{1}{2}, k} \int_{K_y^j} \phi_k(\mathbf{y}) \mu(\mathbf{y}) d\mathbf{y}. \end{aligned} \tag{9}$$

We use the same notations for quadrature rule as in Section 3.1. Let $\mathbf{B} \in \mathbb{R}^{N_y \times N}$ be the matrix representing the integrals over stochastic faces of the basis functions

weighted by the density functions:

$$\mathbf{B}_{j,k} = \int_{K_y^j} \phi_k(\mathbf{y}) \mu(\mathbf{y}) d\mathbf{y} \approx \sum_m \phi_k(\hat{\mathbf{y}}_m) \mu(\hat{\mathbf{y}}_m) w_m. \quad (10)$$

This allows us to trade the online cost of a high-dimensional stochastic integral for offline computations of integrals of reduced stochastic basis functions.

For each spatial interface between neighboring cells, denote N_q as the number of quadrature nodes per stochastic cell, the total number of quadrature nodes along such spatial interface becomes $N_q N_y$, which is typically large. We use a least-squares approximation [31, 32] to determine the coefficients $\mathbf{c}_{i\pm\frac{1}{2},k}$ of the reduced stochastic basis flux approximation. Instead of using $\hat{\mathbf{y}}_m$ to refer to a local quadrature node within a stochastic cell, we now introduce \mathbf{y}_l to represent the global l -th quadrature node, where $l = 1, \dots, N_q N_y$.

Recall from (8) that $\tilde{\mathbf{F}}_{i\pm\frac{1}{2},j}(\mathbf{y})$ represent the reconstructed flux polynomials that can be evaluated at each quadrature node in $K_x^i \times K_y^j$. To organize these values, we define matrices $\tilde{\mathbf{F}}_{\pm\frac{1}{2}}$ which store the reconstructed flux at all quadrature nodes in $D_x \times D_y$:

$$\left(\tilde{\mathbf{F}}_{\pm\frac{1}{2}}\right)_{l,i} = \tilde{\mathbf{F}}_{i\pm\frac{1}{2},j}(\mathbf{y}_l), \quad l = 1, \dots, N_q N_y, \quad i = 1, \dots, N_x, \quad (11)$$

where j corresponds to the cell index such that N_y^j contains the quadrature node l . We define the corresponding Vandermonde matrix $\mathbf{V} \in \mathbb{R}^{N_q N_y \times N}$ as

$$\mathbf{V}_{l,k} = \phi_k(\mathbf{y}_l). \quad (12)$$

To approximate the values of $\mathbf{c}_{i\pm\frac{1}{2},k}$, we solve a standard linear least square problem:

$$\min_{\mathbf{P} \in \text{span}\{\phi_1, \dots, \phi_N\}} \sum_l \left\| \tilde{\mathbf{F}}_{i\pm\frac{1}{2},j}(\mathbf{y}_l) - \mathbf{P}(\mathbf{y}_l) \right\|_2^2. \quad (13)$$

The analytical solution of the problem above is:

$$\mathbf{P} = \mathbf{V} \mathbf{V}^\dagger \tilde{\mathbf{F}}_{\pm\frac{1}{2}},$$

where \dagger denotes the pseudoinverse. In particular, note that $\mathbf{V}^\dagger \tilde{\mathbf{F}}_{\pm\frac{1}{2}}$ are the coefficients of the solution of (13) in the basis $\phi_k(\mathbf{y})$. Since \mathbf{B} in (10) maps coefficients in the $\phi_k(\mathbf{y})$ basis to integrals over stochastic faces, $\bar{\mathbf{F}}_{\pm\frac{1}{2}}$ in (4) can be approximated as

$$\bar{\mathbf{F}}_{\pm\frac{1}{2}} \approx \left(\mathbf{B} \mathbf{V}^\dagger \tilde{\mathbf{F}}_{\pm\frac{1}{2}} \right)^T. \quad (14)$$

This formulation enables us to approximate the solutions in (4) by solving the reduced-order interpolation-based model

$$\mathbf{M} \frac{d\mathbf{U}}{dt} + \left(\mathbf{B}\mathbf{V}^\dagger \tilde{\mathbf{F}}_{+\frac{1}{2}} - \mathbf{B}\mathbf{V}^\dagger \tilde{\mathbf{F}}_{-\frac{1}{2}} \right)^T = \mathbf{0}. \quad (15)$$

Note that even with a reduced basis approach, the dimensions of \mathbf{V} and $\tilde{\mathbf{F}}_{\pm\frac{1}{2}}$ still scale with the size of the stochastic space. As a result, the computational cost of (15) does not necessarily decrease compared to the full SFV method.

4.2 Q-DEIM hyper-reduction

To scale the dimensions of \mathbf{V} and $\tilde{\mathbf{F}}_{\pm\frac{1}{2}}$ with the number of reduced basis, a further step of hyper-reduction on (15) is performed to select a reduced set of interpolation points from Q-DEIM [26].

Specifically, given \mathbf{V} in (12), we obtain a permutation vector $\boldsymbol{\pi}$ from the QR factorization of \mathbf{V}^T . Subsequently, we pick N_H leading entries of $\boldsymbol{\pi}$ and denote them as

$$\mathcal{I} = \boldsymbol{\pi}[1 : N_H].$$

In this way, \mathcal{I} picks the leading rows of \mathbf{V} that are most significant with largest norm. We then obtain a hyper-reduced version of (15):

$$\mathbf{M} \frac{d\mathbf{U}}{dt} + \left(\mathbf{B}\mathbf{V}[\mathcal{I}, :]^\dagger \tilde{\mathbf{F}}_{+\frac{1}{2}}[\mathcal{I}, :] - \mathbf{B}\mathbf{V}[\mathcal{I}, :]^\dagger \tilde{\mathbf{F}}_{-\frac{1}{2}}[\mathcal{I}, :] \right)^T = \mathbf{0}. \quad (16)$$

To summarize, in the full SFV method, a total number of $N_q N_y$ quadrature points are used on each physical interface to evaluate the flux integrals over the stochastic cells. In the ROM, we interpolate the fluxes over all available quadrature points with N reduced basis functions and approximate each flux integral over the stochastic cells with some linear combination of the integrals of these N interpolation bases. In the hyper-reduced ROM, we use Q-DEIM to select a subset of N_H interpolation points from the full set in ROM. In each time-step, all flux integrals can therefore be efficiently approximated by evaluating the nonlinear fluxes only at these N_H selected interpolation points to compute the corresponding interpolation coefficients.

4.3 Choice of reduced stochastic basis

Our hyper-reduced model should work with any choice of reduced stochastic basis as long as it is numerically stable (for example, we could use a polynomial basis in stochastic space). For this work, we utilize a non-intrusively constructed reduced stochastic basis using POD [33, 34].

Recall that $\tilde{\mathbf{F}}_{\pm\frac{1}{2}}$ store the reconstructed flux at all quadrature nodes, as defined in (11). Now, let $\tilde{\mathbf{F}}_{\pm\frac{1}{2}, p} \in \mathbb{R}^{N_q N_y \times N_x}$ represent the reconstructed flux of the p th solution component of the conservation laws. Then, for a set of equally spaced time frames

$[t_1, \dots, t_m]$, we construct

$$\begin{aligned} \left(\tilde{\mathbf{F}}_{\text{snap}}\right)_{\pm\frac{1}{2}} &= \left[\tilde{\mathbf{F}}_{\pm\frac{1}{2},1}(t_1) \dots \tilde{\mathbf{F}}_{\pm\frac{1}{2},n}(t_1) \dots \tilde{\mathbf{F}}_{\pm\frac{1}{2},1}(t_m) \dots \tilde{\mathbf{F}}_{\pm\frac{1}{2},n}(t_m)\right], \\ \tilde{\mathbf{F}}_{\text{snap}} &= \left[\left(\tilde{\mathbf{F}}_{\text{snap}}\right)_{+\frac{1}{2}} \quad \left(\tilde{\mathbf{F}}_{\text{snap}}\right)_{-\frac{1}{2}}\right] \in \mathbb{R}^{N_q N_y \times 2mn N_x}. \end{aligned} \quad (17)$$

The reduced basis can be obtained by computing a singular value decomposition (SVD):

$$\tilde{\mathbf{F}}_{\text{snap}} = \mathbf{U}_S \mathbf{\Sigma} \mathbf{V}_S,$$

where we choose first N left singular vector modes as our reduced basis. The Vandermonde matrix becomes

$$\mathbf{V} = \mathbf{U}_S[:, 1 : N].$$

We observe that $\tilde{\mathbf{F}}_{i\pm\frac{1}{2},j}(\mathbf{y})$ are identical to $\tilde{\mathbf{F}}_{(i\pm 1)\mp\frac{1}{2},j}(\mathbf{y})$ except at the boundaries of D_x . Consequently, redundant flux snapshots can be omitted to reduce memory usage. Additionally, the randomized SVD [35, 36] can be employed for further memory efficiency. Instead of performing a full SVD on the snapshot matrix, randomized SVD first projects the data onto a lower-dimensional subspace using a random sampling matrix, capturing the dominant column space with high probability. The SVD is then performed on this much smaller projected matrix, significantly reducing both memory usage and computational cost.

All results presented on this work use identical stochastic basis functions shared across all physical interfaces for efficiency. However, using locally adaptive stochastic bases could further improve accuracy near shocks, as demonstrated in some adaptive ROM frameworks [37].

4.4 Non-intrusive construction of reduced stochastic basis

A key aspect of the approach presented in this paper is that the reduced stochastic basis can be constructed without needing to directly evaluate the full high-dimensional SFV model. In other words, the reduced stochastic basis can be constructed purely by sampling the one-dimensional spatial model at various parameter values. The process of non-intrusively constructing the reduced stochastic basis is straightforward if the reduced stochastic basis is deterministic (e.g., a high order polynomial basis), but can also be done for a data-driven basis such as POD. We outline the process below.

To collect the flux snapshots used in constructing the POD basis, we may solve the full system (4) using any of the reconstruction methods described above. Since the reconstructed fluxes at global quadrature points are explicitly computed at each time step, they can be directly assembled into the snapshot matrix $\tilde{\mathbf{F}}_{\text{snap}}$ in (17). Alternatively, one can store the solution states $\mathbf{U}(t_1), \dots, \mathbf{U}(t_m)$ and later apply reconstruction to these snapshots to recover the corresponding fluxes, which are then used to form $\tilde{\mathbf{F}}_{\text{snap}}$.

However, the snapshot collection method above results in an intrusive construction that requires the computation of a full high-dimensional solution. In contrast, we

propose a non-intrusive construction by constructing the reduced stochastic basis through a set of decoupled, one-dimensional simulations — one at each stochastic quadrature point \mathbf{y}_l . Specifically, we use the standard FVM to solve:

$$\begin{aligned}\partial_t \mathbf{u} + \nabla_x \cdot \mathbf{F}(\mathbf{u}, \mathbf{y}_l) &= \mathbf{0}, & x \in D_x \subset \mathbb{R}, & \quad t > 0; \\ \mathbf{u}(x, 0, \mathbf{y}_l) &= \mathbf{u}_0(x, \mathbf{y}_l), & x \in D_x \in \mathbb{R}.\end{aligned}$$

Flux snapshots (17) are then collected at the spatial interfaces $i \pm \frac{1}{2}$ using reconstruction on solution snapshots.

One might notice such sampling can already provide complete UQ estimates, as it effectively resolves the stochastic dependence by sampling at every quadrature point. However, one of the main advantages of this framework is its flexibility in choosing how the stochastic space is sampled when constructing the reduced stochastic basis. Instead of sampling all quadrature points, one could select a subset based on sparse grid rules [38, 39] or other adaptive strategies [40, 41], potentially reducing the number of one-dimensional simulations while maintaining sufficient accuracy for UQ purposes.

5 Numerical experiments

In this section, we present numerical experiments to assess the performance of our proposed method for uncertainty quantification across different stochastic dimensions. We consider the one-dimensional Burgers' and compressible Euler equations. We first compare the performance of the two proposed WENO reconstruction procedures, and then evaluate the ROM performance.

5.1 Preliminaries

We choose $\widehat{\mathbf{F}}$ to be the Lax-Friedrich flux [42] which, for reconstructed left and right states $\tilde{\mathbf{u}}_L, \tilde{\mathbf{u}}_R$, is defined as

$$\widehat{\mathbf{F}}(\tilde{\mathbf{u}}_L, \tilde{\mathbf{u}}_R) = \frac{1}{2} (\mathbf{F}(\tilde{\mathbf{u}}_L) + \mathbf{F}(\tilde{\mathbf{u}}_R)) - \frac{\lambda}{2} (\tilde{\mathbf{u}}_R - \tilde{\mathbf{u}}_L),$$

where λ represents the local maximum wave speed following the Davis wave speed formulation [43].

On a one-dimensional reference domain $[-1, 1]$, the two-point Gaussian quadrature rule approximates integrals via

$$\int_{-1}^1 f(\mathbf{u}) d\mathbf{y} \approx w_1 f(y_1) + w_2 f(y_2),$$

where the quadrature nodes and weights are given by

$$y_1 = -1/\sqrt{3}, \quad y_2 = 1/\sqrt{3}, \quad w_1 = w_2 = 1.$$

For higher-dimensional stochastic integrals, the quadrature rule is constructed as a tensor-product extension of the one-dimensional case. The number of quadrature points in this rule is $N_q = 2^q$, where q denotes the dimension of the stochastic space.

To assess errors of our ROMs, we report the relative L_1 norm of the difference between the expected value of the simulated stochastic ROM solutions and that of the reference solution obtained from full SFV method via WENO with reconstructed states or with reconstructed fluxes. The reference solutions are computed on a refined grid consisting of N_x physical volumes, where the fluxes at each interface are evaluated using a total of $N_q N_y$ quadrature points in the stochastic space. Denote $\mathbf{U} \subset \mathbb{R}^{N_x \times N_q N_y \times n}$ as the computed solutions (cell averages) and denote $\mathbf{U}_{\text{ref}} \subset \mathbb{R}^{N_x \times N_q N_y \times n}$ as the corresponding reference solution. Using two-point Gaussian quadrature rule and uniform grid, the relative L_1 error simplifies to

$$\|\mathbf{U} - \mathbf{U}_{\text{ref}}\|_{L_1}^{\text{rel}} = \frac{\sum_{i,j,p} |(\mathbf{U} - \mathbf{U}_{\text{ref}})_{i,j,p}|}{\sum_{i,j,p} |(\mathbf{U}_{\text{ref}})_{i,j,p}|},$$

where p indexes the solution components.

For all simulations, we use MATLAB's adaptive ODE45 solver with a relative error tolerance of 1e-6 and an absolute error tolerance of 1e-8. The reported runtime is measured using the `timeit` function applied to the solver. The MATLAB version used is R2024a.

5.2 Burgers' equation

N_y	Difference	Runtime (s) (state)	Runtime (s) (flux)
4^2	1.09e-2	7.39e-2	4.82e-2
8^2	6.84e-3	2.89e-1	1.68e-1
16^2	2.99e-3	2.34e0	1.12e0
32^2	1.14e-3	8.69e0	5.08e0
64^2	3.81e-4	7.13e1	7.61e1

Table 1: Burgers' equation: Relative difference between WENO with reconstructed states and WENO with reconstructed fluxes, along with their total time-stepping runtimes

The first equation we test is Burgers' equation:

$$\begin{aligned} \frac{\partial U}{\partial t} + \frac{\partial f(U)}{\partial x} &= 0, \quad x \in [0, 1], \\ U_0(x, y_1, y_2) &= \sin(2\pi x) + 0.5 \sin(2\pi y_1) + y_2, \end{aligned} \tag{18}$$

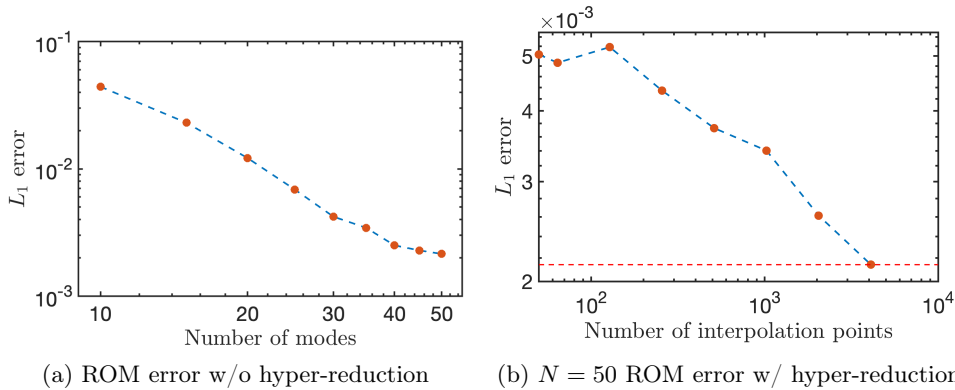


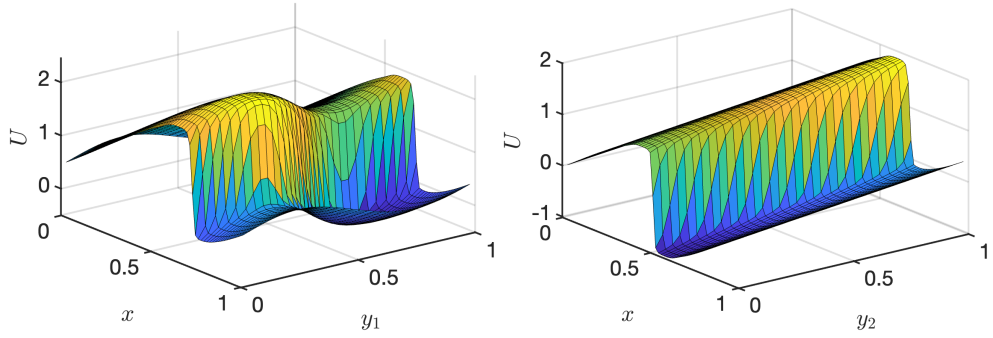
Fig. 1: Error plots for the Burgers' equation ROM showing (a) variation with the number of modes and (b) variation with the number of interpolation nodes at fixed $N = 50$. The red dashed line in (b) indicates the error from plot (a) for $N = 50$ modes.

where $y_1, y_2 \sim \mathcal{U}[0, 1]$. We impose periodic boundary conditions in the spatial domain D_x and outflow boundary condition in the stochastic domain D_y . The simulation is run until the final time $T = 0.2$, when the solution develops a shock propagating towards the right. Note that uncertainty is introduced in both the amplitude of the initial sine wave and the shock speed.

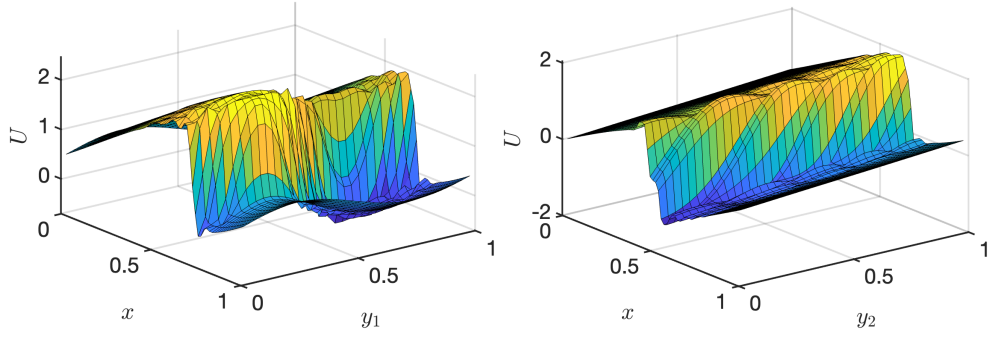
We apply the full SFV method to solve the problem using both WENO reconstruction procedures described in Section 3 and report their relative differences in Table 1. In this comparison, we fix $N_x = 64$ and vary N_y . The solution obtained from the procedure of reconstructed states is taken as a reference (as validated in [22, 29]) to assess the accuracy of the procedure of reconstructed fluxes. By refining the stochastic grid, we can verify that WENO with reconstructed fluxes achieves similar accuracy. We also report the total time-stepping runtime in Table 1. WENO with reconstructed fluxes remains faster up to $N_y = 64^2$, where flux evaluations are no longer the dominant cost, and it requires approximately 20% more time steps than WENO with reconstructed states. We note that the implementation is not fully optimized, and further performance improvements are possible.

Next, we evaluate the performance of the ROM. We fix $N_x = 64$ and $N_y = 32^2$. First, we plot the error between SFV method with reconstruction of flux and the ROM for different numbers of modes in Figure 1a, observing that the error decreases as N increases. Then, we fix $N = 50$ and vary $N_H \geq N$ to assess the accuracy of hyper-reduction in Figure 1b, where we observe a convergence of error as N_H increases. Although increasing N_H can further reduce the error, the results with $N_H = N$ already achieves a reasonable level of accuracy while providing a substantial reduction in computational cost. This demonstrates that the chosen hyper-reduction level $N_H = N$ provides a good balance between accuracy and efficiency.

Finally, we plot the solution U at the final time for both WENO with reconstructed fluxes and ROM at $y_1 = 1$ and $y_2 = 1$ in Figure 2. Here we set $N_H = N$ and consider $N_H = N = 10$ and $N_H = N = 20$. Next, we plot the solution means and standard

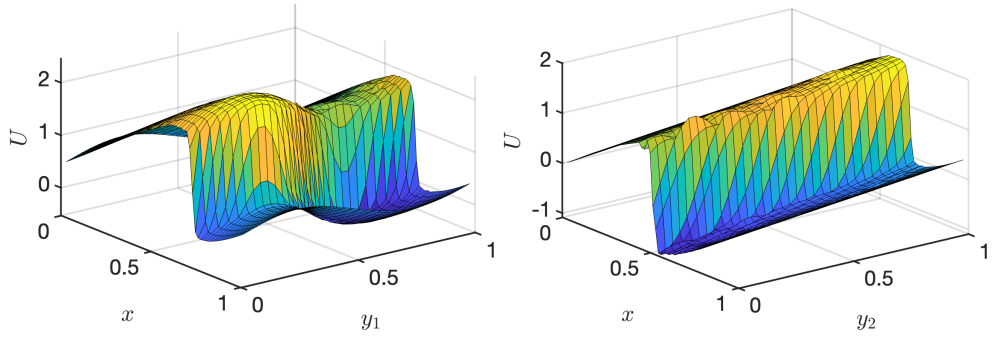


(a) WENO with reconstructed fluxes, $y_2 = 1$ (b) WENO with reconstructed fluxes, $y_1 = 1$



(c) $N = 10$ ROM, $y_2 = 1$

(d) $N = 10$ ROM, $y_1 = 1$



(e) $N = 20$ ROM, $y_2 = 1$

(f) $N = 20$ ROM, $y_1 = 1$

Fig. 2: Solution plots at $y_1 = 1$ or $y_2 = 1$ for Burgers' equation ($N_H = N$).

deviations for these two mode choices in [Figure 3](#). We observe oscillations around shocks for ROM at $N = 10$, which diminishes as N increases to 20. Similar oscillations appear in the solution mean and standard deviation at $N = 10$, but they are also reduced at $N = 20$.

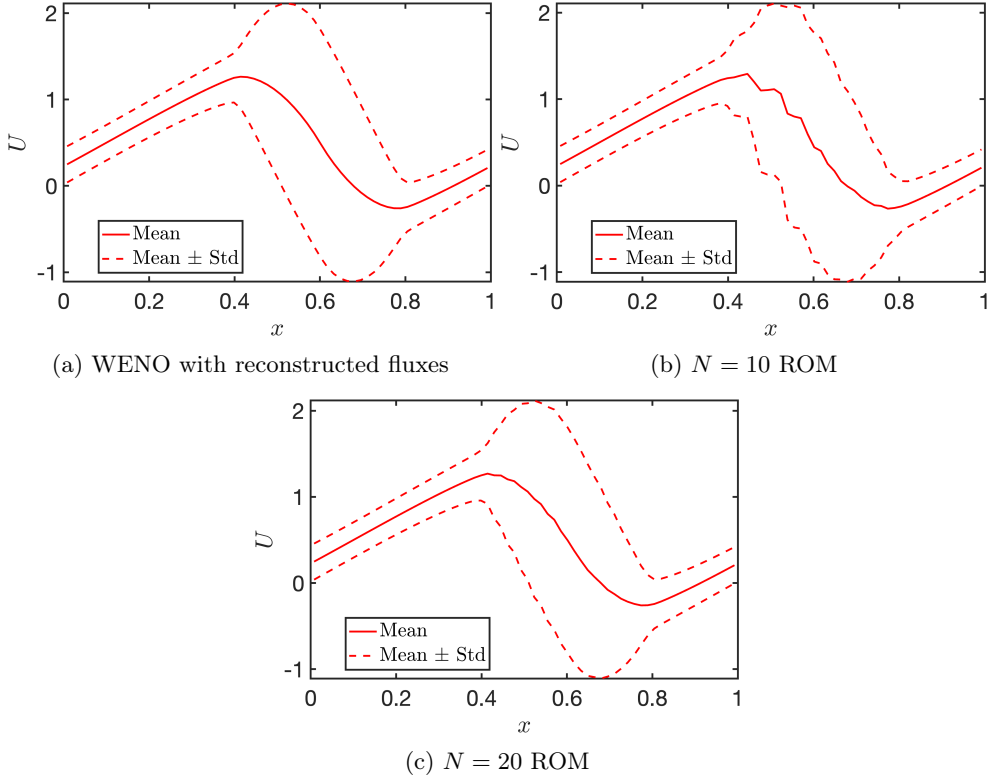


Fig. 3: Solution mean and mean \pm std for Burgers' equation ($N_H = N$).

5.3 Compressible Euler equations

We now test the one-dimensional compressible Euler equations:

$$\begin{aligned}
 \frac{\partial \mathbf{U}}{\partial t} + \frac{\partial \mathbf{F}(\mathbf{U})}{\partial x} &= 0, \quad x \in [0, 1], \\
 \mathbf{U} &= [\rho, \rho u, E]^T, \quad \mathbf{F} = [\rho u, \rho u^2 + p, u(E + p)]^T, \\
 p &= (\gamma - 1) \left(E - \frac{1}{2} \rho u^2 \right).
 \end{aligned} \tag{19}$$

We first consider the Sod shock tube problem [44] with uncertainty in the shock position:

$$\mathbf{W}_0(x, y) = [\rho_0, u_0, p_0]^T = \begin{cases} [1.0, 0.0, 1.0]^T & x < 0.475 + 0.05y, \\ [0.125, 0.0, 0.1]^T & x > 0.475 + 0.05y, \end{cases}$$

N_y	Difference	Runtime (s) (state)	Runtime (s) (flux)
4	7.12e-4	6.47e0	1.59e-1
8	3.73e-4	1.21e0	2.59e-1
16	1.26e-4	8.38e-1	4.82e-1
32	6.31e-5	1.56e0	1.01e0
64	3.15e-5	5.24e0	2.83e0

Table 2: Sod shock tube: Relative difference between WENO with reconstructed states and WENO with reconstructed fluxes, along with their total time-stepping runtimes

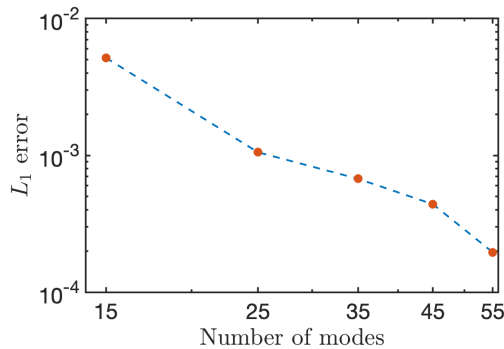
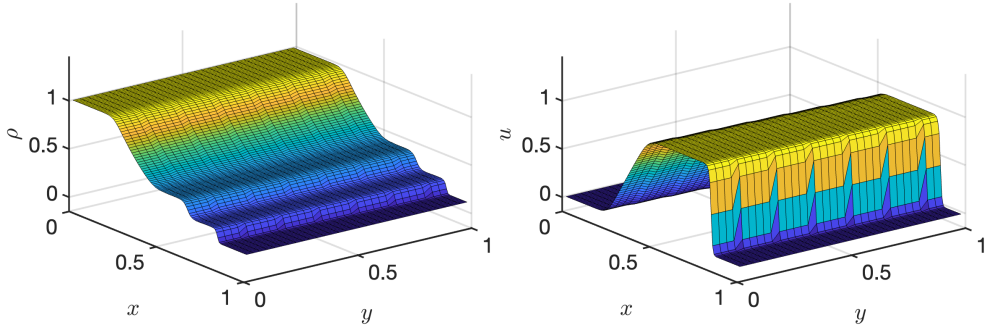


Fig. 4: ROM error w/o hyper-reduction in stochastic Sod shock problem.

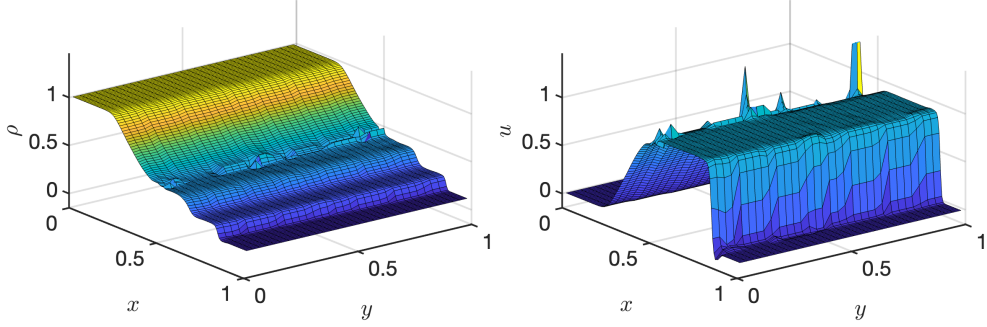
where $y \sim \mathcal{U}[0,1]$ and we set $\gamma = 1.4$. The simulation is run until the final time $T = 0.2$. This problem setting was first considered for the SFV method in Sec 3.3.2 of [29].

In Table 2, we fix $N_x = 128$ and vary N_y to again compare the relative differences between the two WENO reconstruction procedures. We continue to observe similar accuracy. We also compare their total runtime for time-stepping. WENO with reconstructed fluxes consistently achieves faster runtimes across all cases. However, WENO with reconstructed states exhibits noticeably longer runtimes for small N_y compared with larger N_y . This is because it requires much smaller time-step sizes to maintain positivity. For example, WENO with reconstructed states takes approximately 133% more time steps for $N_y = 4$ than for $N_y = 16$. WENO with reconstructed states also takes 156% more adaptive time-steps than WENO with reconstructed fluxes for $N_y = 4$.

Now we fix $N_x = 128$ and $N_y = 32$. We first assess the performance of the ROM in the absence of hyper-reduction. Consistent with earlier analysis, the ROM error is evaluated with respect to the SFV solution obtained via WENO with reconstructed fluxes. We vary the number of modes and plot the errors in Figure 4, where we observe a convergence of error as N increases. Next, we visualize the density ρ and velocity u

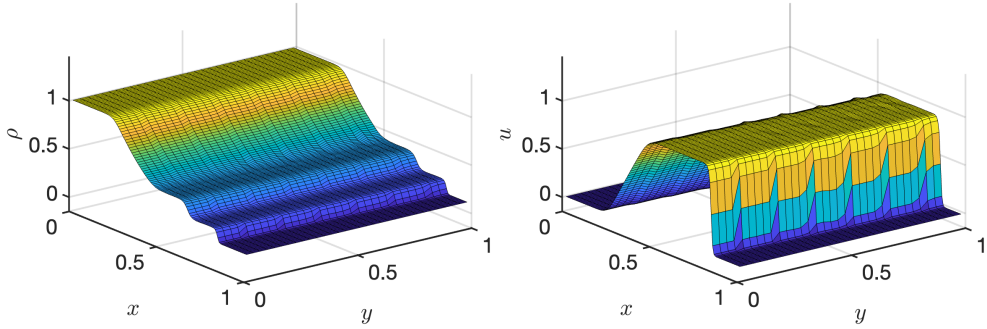


(a) ρ plot, WENO with reconstructed fluxes (b) u plot, WENO with reconstructed fluxes



(c) ρ plot, $N = 15$ ROM

(d) u plot, $N = 15$ ROM



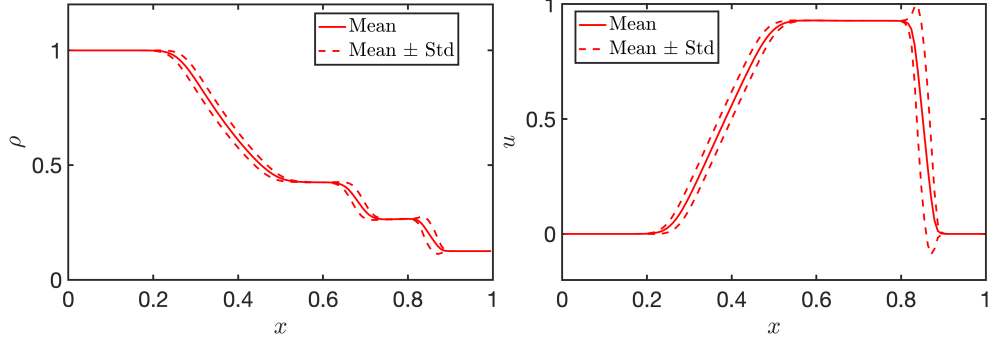
(e) ρ plot, $N = 30$ ROM

(f) u plot, $N = 30$ ROM

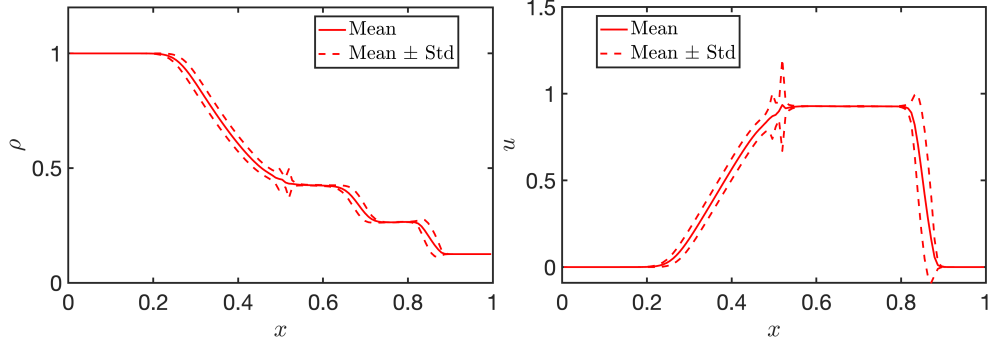
Fig. 5: Solution plots for stochastic Sod shock tube problem without hyper-reduction.

for mode numbers $N = 5$ and $N = 30$ in Figure 5. We observe oscillations at $N = 15$ but they diminish as N increases to 30. Finally, we plot the mean and standard deviation for ρ and u in Figure 6. We again observe oscillations in solution means for $N = 15$ and smooth solution means for $N = 30$.

For this setup, we notice that hyper-reduction can lead to time-stepping failures when using a small number of modes. Therefore, we test hyper-reduction for $N_H =$

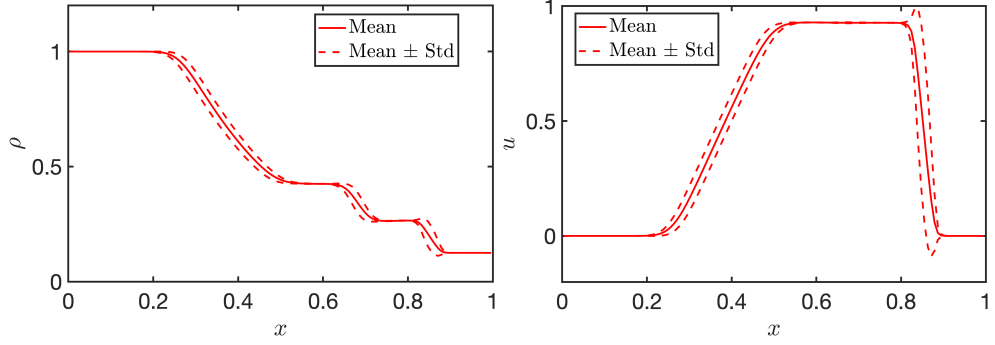


(a) Mean \pm std of ρ , WENO with reconstructed fluxes (b) Mean \pm std of u , WENO with reconstructed fluxes



(c) Mean \pm std of ρ , $N = 15$ ROM

(d) Mean \pm std of u , $N = 15$ ROM



(e) Mean \pm std of ρ , $N = 30$ ROM

(f) Mean \pm std of u , $N = 30$ ROM

Fig. 6: Solution mean and mean \pm std for stochastic Sod shock tube problem without hyper-reduction.

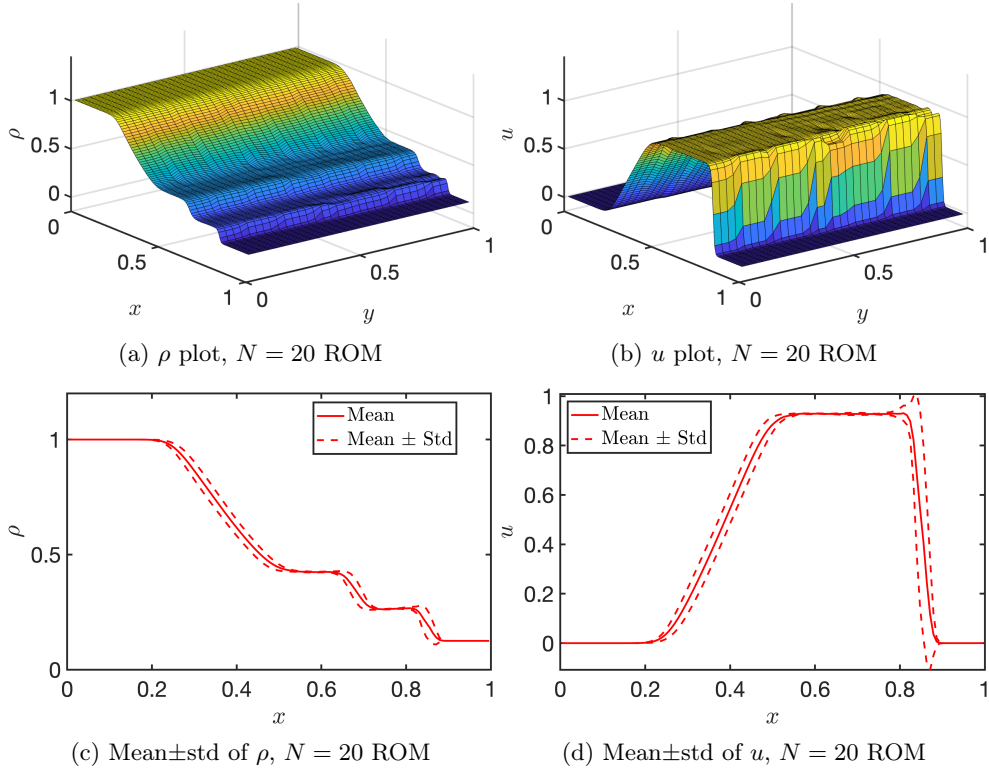


Fig. 7: Solution plots and mean \pm std for stochastic Sod shock tube with hyper-reduction $N_H = N = 20$.

$N = 20$ with plots in [Figure 7](#). We observe some oscillations smaller than the $N = 15$ case without hyper-reduction.

Lastly, we test a wider range of uncertainty in initial conditions:

$$\mathbf{W}_0(x, y) = [\rho_0, u_0, p_0]^T = \begin{cases} [1.0, 0.0, 1.0]^T & x < 0.3 + 0.3y, \\ [0.125, 0.0, 0.1]^T & x > 0.3 + 0.3y, \end{cases}$$

where we keep other parameters same as before. In this setting, we observe that WENO with reconstructed states suffers from preserving positivity, while WENO with reconstructed fluxes remains robust. In [Figure 8](#), we again plot the density ρ and velocity u computed using WENO with reconstructed fluxes, along with the corresponding results from $N = 40$ ROM without hyper-reduction.

6 Summary and future work

In this work, we introduce an interpolation-based reduced-order model for dimensionality reduction of the SFV method, designed to solve uncertainty quantification

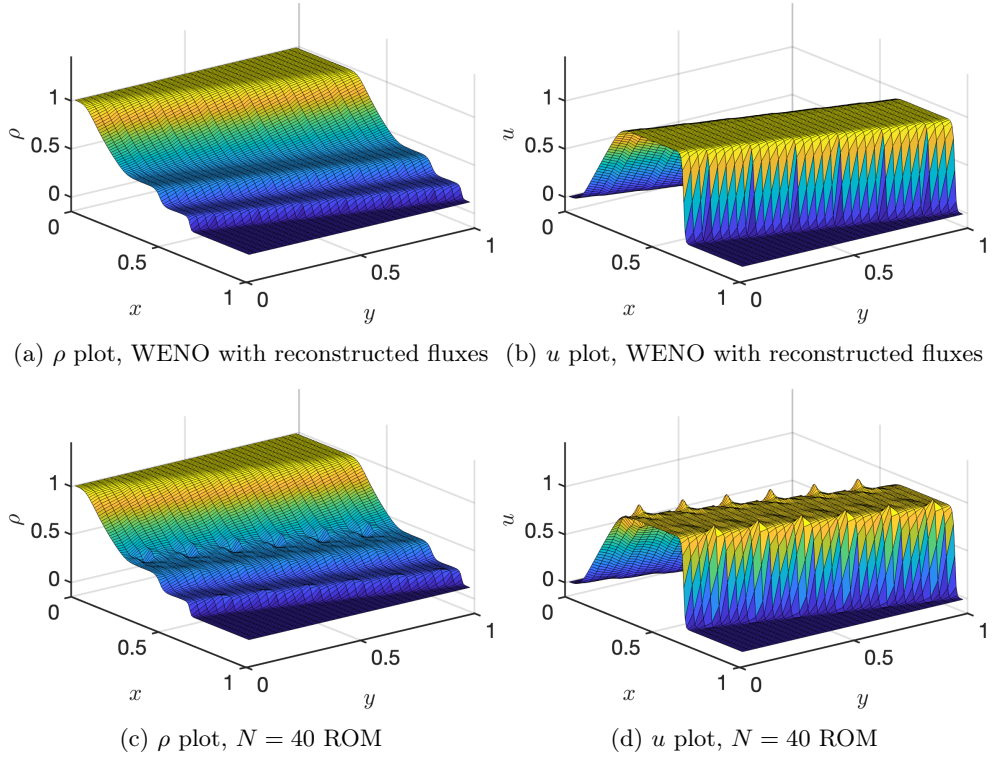


Fig. 8: Solution plots for stochastic Sod shock tube without hyper-reduction (initial condition with wider range of shock positions)

problems in systems of conservation laws. The model approximates flux integrals using a global stochastic POD basis, enabling efficient offline integration of basis functions while computing only the coefficients during the online stage. Additional computational savings are achieved through Q-DEIM hyper-reduction, which selects a subset of interpolation points from the full quadrature grid. We also propose a non-intrusive approach for constructing the snapshot matrix by solving multiple 1D problems using the standard FV method. Together, these techniques provide a scalable and accurate framework for uncertainty quantification.

In future work, we aim to enhance the accuracy of the reduced-order model and extend its formulation to conservation laws in two- and three-dimensional physical domains. For example, while we use one set of reduced stochastic basis for all spatial points in this work, different sets of reduced stochastic bases could be computed independently at each spatial coordinate. This would adapt the dimension of the reduced stochastic basis to the stochastic solution at different spatial points, potentially improving accuracy.

Declarations

Ethical Approval

Not applicable.

Funding

Ray Qu and Jesse Chan gratefully acknowledge support from National Science Foundation under award DMS-1943186. Jesse Chan additionally acknowledges support from the National Science Foundation under award DMS-2231482. Svetlana Tokareva gratefully acknowledges the support of the NNSA through the Laboratory Directed Research and Development (LDRD) program at Los Alamos National Laboratory under project number 20250032DR. Los Alamos National Laboratory is operated by Triad National Security, LLC for the U.S. Department of Energy's NNSA. The Los Alamos unlimited release number is LA-UR-25-24954.

Availability of data and materials

All simulation codes used in this work are publicly available at: https://github.com/rayqu1126/SFV_ROM/releases/tag/v1.0. The code repository is also archived at: <https://doi.org/10.5281/zenodo.17517369>. Data supporting the results are available upon request.

References

- [1] LeVeque, R.: Numerical Methods for Conservation Laws. Birkhäuser Verlag, Basel (1992)
- [2] Godlewski, E., Raviart, P.-A.: Numerical Approximation of Hyperbolic Systems of Conservation Laws, 1st edn., p. 510. Springer, New York, NY (1996). <https://doi.org/10.1007/978-1-4612-0713-9>
- [3] Morton, K., Sonar, T.: Finite volume methods for hyperbolic conservation laws. *Acta Numerica* **16**, 155–238 (2007)
- [4] Krivodonova, L., Xin, J., Remacle, J.-F., Chevaugeon, N., Flaherty, J.E.: Shock detection and limiting with discontinuous Galerkin methods for hyperbolic conservation laws. *Applied Numerical Mathematics* **48**(3-4), 323–338 (2004) <https://doi.org/10.1016/j.apnum.2003.11.002>
- [5] Cockburn, B., Shu, C.-W.: Runge-Kutta Discontinuous Galerkin Methods for Convection-Dominated Problems. *Journal of Scientific Computing* **16**(3), 173–261 (2001) <https://doi.org/10.1023/A:1012873910884>
- [6] Hesthaven, J.S., Warburton, T.: Nodal Discontinuous Galerkin Methods: Algorithms, Analysis, and Applications. Texts in Applied Mathematics, vol. 54. Springer, New York, NY (2007). <https://doi.org/10.1007/978-0-387-72067-8>
- [7] Toro, E.F.: Riemann Solvers and Numerical Methods for Fluid Dynamics. Springer, Heidelberg (2009). <https://doi.org/10.1007/b79761>
- [8] Dafermos, C.M.: Hyperbolic Conservation Laws in Continuum Physics vol. 325, 4th edn. Springer, Berlin, Heidelberg (2016). <https://doi.org/10.1007/978-3-662-49451-6>
- [9] Mishra, S., Schwab, C.: Sparse tensor multi-level Monte Carlo finite volume methods for hyperbolic conservation laws with random initial data. *Math. Comp.* **81**, 1979–2018 (2012) <https://doi.org/10.1090/S0025-5718-2012-02574-9>
- [10] Mishra, S., Schwab, C., Šukys, J.: Multi-level Monte Carlo finite volume methods for nonlinear systems of conservation laws in multi-dimensions. *Journal of Computational Physics* **231**(8), 3365–3388 (2012) <https://doi.org/10.1016/j.jcp.2012.01.011>
- [11] Poëtte, G., Després, B., Lucor, D.: Uncertainty quantification for systems of conservation laws. *Journal of Computational Physics* **228**(7), 2443–2467 (2009) <https://doi.org/10.1016/j.jcp.2008.12.018>
- [12] Lin, G., Su, C.-H., Karniadakis, G.E.: Predicting shock dynamics in the presence of uncertainties. *Journal of Computational Physics* **217**(1), 260–276 (2006) <https://doi.org/10.1016/j.jcp.2005.08.011>

[//doi.org/10.1016/j.jcp.2006.02.009](https://doi.org/10.1016/j.jcp.2006.02.009)

- [13] Lin, G., Su, C.-H., Karniadakis, G.E.: Stochastic modeling of random roughness in shock scattering problems: Theory and simulations. *Computer Methods in Applied Mechanics and Engineering* **197**(43), 3420–3434 (2008) <https://doi.org/10.1016/j.cma.2008.02.025>
- [14] Tryoen, J., Le Maître, O., Ndjinga, M., Ern, A.: Roe solver with entropy corrector for uncertain hyperbolic systems. *Journal of Computational and Applied Mathematics* **235**(2), 491–506 (2010) <https://doi.org/10.1016/j.cam.2010.05.043>
- [15] Herty, M., Kolb, A., Müller, S.: Multiresolution analysis for stochastic hyperbolic conservation laws. *IMA Journal of Numerical Analysis* **44**(1), 536–575 (2023) <https://doi.org/10.1093/imanum/drad010>
- [16] Tryoen, J., Le Maître, O., Ndjinga, M., Ern, A.: Intrusive Galerkin methods with upwinding for uncertain nonlinear hyperbolic systems. *Journal of Computational Physics* **229**(18), 6485–6511 (2010) <https://doi.org/10.1016/j.jcp.2010.05.007>
- [17] Gottlieb, D., Xiu, D.: Galerkin method for wave equations with uncertain coefficients. *Commun. Comput. Phys.* **3**, 505–518 (2008)
- [18] Reagan, M.T., Najm, H.N., Ghanem, R.G., Knio, O.M.: Uncertainty quantification in reacting-flow simulations through non-intrusive spectral projection. *Combustion and Flame* **132**(3), 545–555 (2003) [https://doi.org/10.1016/S0010-2180\(02\)00503-5](https://doi.org/10.1016/S0010-2180(02)00503-5)
- [19] Berveiller, M., Sudret, B., Lemaire, M.: Stochastic finite element: a non intrusive approach by regression. *European Journal of Computational Mechanics* **15**(1-3), 81–92 (2006) <https://doi.org/10.3166/remn.15.81-92>
- [20] Hosder, S., Walters, R.: Non-Intrusive Polynomial Chaos Methods for Uncertainty Quantification in Fluid Dynamics. <https://doi.org/10.2514/6.2010-129>
- [21] Le Maître, O.P., Knio, O.M.: Galerkin Methods, pp. 73–105. Springer, Dordrecht (2010). https://doi.org/10.1007/978-90-481-3520-2_4
- [22] Tokareva, S., Schwab, C., Mishra, S.: High Order SFV and Mixed SDG/FV Methods for the Uncertainty Quantification in Multidimensional Conservation Laws. In: High Order Nonlinear Numerical Schemes for Evolutionary PDEs, pp. 109–133. Springer, Cham (2014). https://doi.org/10.1007/978-3-319-05455-1_7
- [23] Harmon, J.J., Tokareva, S., Zlotnik, A., Swart, P.J.: Adaptive uncertainty quantification for stochastic hyperbolic conservation laws. *SIAM/ASA Journal on Uncertainty Quantification* **13**(2), 339–374 (2025) <https://doi.org/10.1137/23M1624750>

- [24] Walton, S., Tokareva, S., Manzini, G.: The Tensor-Train Stochastic Finite Volume Method for Uncertainty Quantification (2024). <https://arxiv.org/abs/2404.06574>
- [25] Chaturantabut, S., Sorensen, D.C.: Nonlinear Model Reduction via Discrete Empirical Interpolation. *SIAM Journal on Scientific Computing* **32**(5), 2737–2764 (2010) <https://doi.org/10.1137/090766498>
- [26] Drmač, Z., Gugercin, S.: A New Selection Operator for the Discrete Empirical Interpolation Method—Improved A Priori Error Bound and Extensions. *SIAM Journal on Scientific Computing* **38**(2), 631–648 (2016) <https://doi.org/10.1137/15M1019271>
- [27] Liu, X.-D., Osher, S., Chan, T.: Weighted Essentially Non-oscillatory Schemes. *Journal of Computational Physics* **115**(1), 200–212 (1994) <https://doi.org/10.1006/jcph.1994.1187>
- [28] Titarev, V.A., Toro, E.F.: Finite-volume WENO schemes for three-dimensional conservation laws. *Journal of Computational Physics* **201**(1), 238–260 (2004) <https://doi.org/10.1016/j.jcp.2004.05.015>
- [29] Abgrall, R., Tokareva, S.: *The Stochastic Finite Volume Method*, pp. 1–57. Springer, Cham (2017). https://doi.org/10.1007/978-3-319-67110-9_1
- [30] Courant, R., Friedrichs, K., Lewy, H.: On the partial difference equations of mathematical physics. *IBM Journal of Research and Development* **11**(2), 215–234 (1967) <https://doi.org/10.1147/rd.112.0215>
- [31] Bjerhammar, A.: Application of calculus of matrices to method of least squares : with special reference to geodetic calculations. (1951)
- [32] Björck: Least squares methods. *Handbook of Numerical Analysis*, vol. 1, pp. 465–652. Elsevier (1990). [https://doi.org/10.1016/S1570-8659\(05\)80036-5](https://doi.org/10.1016/S1570-8659(05)80036-5)
- [33] Charatterjee, A.: An introduction to the proper orthogonal decomposition. *Current Science* **78**, 808–817 (2000)
- [34] Liang, Y.C., P., L.H., Lim, S.P., Lin, W.Z., Lee, K.H., Wu, C.G.: Proper Orthogonal Decomposition and Its Applications—Part I: Theory. *Journal of Sound and Vibration* **252**, 527–544 (2002) <https://doi.org/10.1006/jsvi.2001.4041>
- [35] Drinea, E., Drineas, P., Huggins, P.: A randomized singular value decomposition algorithm for image processing applications. In: *Proceedings of the 8th Panhellenic Conference on Informatics*, pp. 278–288 (2001)
- [36] Halko, N., Martinsson, P.G., Tropp, J.A.: Finding Structure with Randomness: Probabilistic Algorithms for Constructing Approximate Matrix Decompositions.

- SIAM Review **53**(2), 217–288 (2011) <https://doi.org/10.1137/090771806>
- [37] Amsallem, D., Farhat, C.: Interpolation Method for Adapting Reduced-Order Models and Application to Aeroelasticity. *AIAA Journal* **46**(7), 1803–1813 (2008) <https://doi.org/10.2514/1.35374>
- [38] Ma, X., Zabaras, N.: An adaptive hierarchical sparse grid collocation algorithm for the solution of stochastic differential equations. *Journal of Computational Physics* **228**(8), 3084–3113 (2009) <https://doi.org/10.1016/j.jcp.2009.01.006>
- [39] Xiu, D., Hesthaven, J.S.: High-Order Collocation Methods for Differential Equations with Random Inputs. *SIAM Journal on Scientific Computing* **27**(3), 1118–1139 (2005) <https://doi.org/10.1137/040615201>
- [40] Bui-Thanh, T., Willcox, K., Ghattas, O.: Model Reduction for Large-Scale Systems with High-Dimensional Parametric Input Space. *SIAM Journal on Scientific Computing* **30**(6), 3270–3288 (2008) <https://doi.org/10.1137/070694855>
- [41] Narayan, A., Jakeman, J.D.: Adaptive Leja Sparse Grid Constructions for Stochastic Collocation and High-Dimensional Approximation. *SIAM Journal on Scientific Computing* **36**(6), 2952–2983 (2014) <https://doi.org/10.1137/140966368>
- [42] Lax, P.D.: Weak solutions of nonlinear hyperbolic equations and their numerical computation. *Communications on Pure and Applied Mathematics* **7**(1), 159–193 (1954) <https://doi.org/10.1002/cpa.3160070112>
- [43] Davis, S.F.: Simplified Second-Order Godunov-Type Methods. *SIAM Journal on Scientific and Statistical Computing* **9**(3), 445–473 (1988) <https://doi.org/10.1137/0909030>
- [44] Sod, G.A.: A survey of several finite difference methods for systems of nonlinear hyperbolic conservation laws. *Journal of Computational Physics* **27**(1), 1–31 (1978) [https://doi.org/10.1016/0021-9991\(78\)90023-2](https://doi.org/10.1016/0021-9991(78)90023-2)